



Article

Enhanced Efficiency of MAPbI₃ Perovskite Solar Cells with FAPbX₃ Perovskite Quantum Dots

Lung-Chien Chen ^{1,*}, Ching-Ho Tien ¹, Zong-Liang Tseng ^{2,*} and Jun-Hao Ruan ¹

¹ Department of Electro-Optical Engineering, National Taipei University of Technology, Taipei 10608, Taiwan; chtien@mail.ntut.edu.tw (C.-H.T.); bj031001@gmail.com (J.-H.R.)

² Department of Electronic Engineering and Organic Electronics Research Center, Ming Chi University of Technology, New Taipei City 24301, Taiwan

* Correspondence: ocean@ntut.edu.tw (L.-C.C.); tw78787788@yahoo.com.tw (Z.-L.T.); Tel.: +886-2-27712171 (ext. 4634) (L.-C.C.); +886-2-29089899 (ext. 4866) (Z.-L.T.)

Received: 17 November 2018; Accepted: 14 January 2019; Published: 19 January 2019



Abstract: We describe a method to enhance power conversion efficiency (PCE) of MAPbI₃ perovskite solar cell by inserting a FAPbX₃ perovskite quantum dots (QD-FAPbX₃) layer. The MAPbI₃ and QD-FAPbX₃ layers were prepared using a simple, rapid spin-coating method in a nitrogen-filled glove box. The solar cell structure consists of ITO/PEDOT:PSS/MAPbI₃/QD-FAPbX₃/C₆₀/Ag, where PEDOT:PSS, MAPbI₃, QD-FAPbX₃, and C₆₀ were used as the hole transport layer, light-absorbing layer, absorption enhance layer, and electron transport layer, respectively. The MAPbI₃/QD-FAPbX₃ solar cells exhibit a PCE of 7.59%, an open circuit voltage (Voc) of 0.9 V, a short-circuit current density (Jsc) of 17.4 mA/cm², and a fill factor (FF) of 48.6%, respectively.

Keywords: solar cells; perovskite; quantum dots; MAPbI₃; FAPbX₃

1. Introduction

Hybrid organic-inorganic perovskite materials have been widely accepted and applied in solar cells. The power conversion efficiency has evolved from 3.8% in 2009 to a certified value of 22.7% in 2018 [1–5]. Perovskite materials are a versatile material with unique optoelectronic properties, exhibiting strong light absorption, long diffusion length, and high mobility [6]. Developing high quality perovskite films is critical to improving perovskite solar cell efficiency. It is well known that high-performance solar cells originate from a low absorption bandgap (the optimal absorption band gap around a value of 1.1–1.5 eV) upon solar spectrum [7–9], low exciton binding energy [10,11], and long carrier diffusion length [12]. In addition, perovskite solar cells offer additional characteristics, like thin-film, flexibility, semitransparency, lightweight, and low-costs processing. A significant number of investigations have been focused on perovskite quantum dots (QDs) due to relatively abundant perovskite component sources [13–15]. The perovskite QD material present several advantageous properties, including band engineering through size and composition control, high absorption coefficient, light-response ranges (light absorption over a wide range of wavelengths from UV-visible to near IR), multiple exciton generation, cost-effectiveness, and solution process ability. Consequently, they are regarded as good light harvesters in perovskite solar cells [16–20]. While perovskite solar cells have experienced a steep increase in performance efficiency, they also show great potential to become a low-cost alternative to conventional solar cells. Due to the limited bandgap tunability of the perovskite material, near-infrared photons cannot be effectively captured in standard perovskite absorber layers by perovskite solar cells. We report on a two-step spin-coating perovskite solar cell manufacturing process, in which the MAPbI₃/QD-FAPbX₃ perovskite architecture is formed while using solvent-engineering techniques. Besides, the MAPbI₃/QD-FAPbX₃ layer exhibits a marginally

broad light absorption region; the current density is also prominently enhanced, which is beneficial for improving the power conversion efficiency. These results explain why perovskite solar cells containing FAPbX₃ QDs exhibit a much higher PCE than cells without.

2. Materials and Methods

The 0.2 m mol of FAPbX₃ (X = I, Br) (FAPbBr_{1.5}I_{1.5} and FAPbBrI₂) perovskite QD solution were prepared in this study while using a simple and rapid method. Table 1 shows the FAI (Lumtec Corp., Taipei, Taiwan), FAB (Lumtec Corp., Taipei, Taiwan), PbI₂ (Alfa Aesar, Lancashire, UK), and PbBr₂ (Alfa Aesar, Lancashire, UK) perovskite FAPbX₃ (X = I, Br) QDs solution parameters. The FAB powder, FAI powder, PbI₂ powder, and PbBr₂ powder were decanted into a solution of 2 mL of dimethylformamide (DMF) (Echo Chemical Co., Ltd., Miaoli, Taiwan); and, 300 µL of oleic acid (Echo Chemical Co., Ltd., Miaoli, Taiwan) and 5 µL of n-octylamine (Echo Chemical Co., Ltd., Miaoli, Taiwan) were decanted into this mixture to form the FAPbX₃ (X = I, Br) precursor solution. Subsequently, A 20 µL of FAPbX₃ (X = I, Br) precursor solution was decanted into 2 mL of chlorobenzene (Echo Chemical Co., Ltd., Miaoli, Taiwan) and 3 mL of ethyl acetate (Echo Chemical Co., Ltd., Miaoli, Taiwan), followed by the centrifugal process to separate the red precipitate from the FAPbX₃ (X = I, Br) precursor solution. The said red precipitate was dried under vacuum for 12 h to entirely eliminate the solvent. The FAPbX₃ (X = I, Br) powder was then dissolved in 60 µL of chlorobenzene to prepare the FAPbX₃ (X = I, Br) perovskite QD solution.

Table 1. Parameters of FAPbX₃ (X = I, Br) perovskite quantum dots (QDs) solution.

Material	FAPbBr _{1.5} I _{1.5}	FAPbBrI ₂
FAI	17.1 mg	–
FAB	12.5 mg	25 mg
PbI ₂	46.1 mg	92.2 mg
PbBr ₂	36.7 mg	–

The patterned ITO glass (Ruilong Corp., Miaoli, Taiwan) was cleaned using ultrasonic treatment in deionized (DI) water, acetone, and isopropanol. The ITO glass was then treated in a UV cleaner for 10 min. The cleaned ITO glass was coated with a PEDOT:PSS solution (UMAT Corp., Hsinchu, Taiwan) using a spin-coating method at 4000 rpm for 30 s, followed by heating at 120 °C for 10 min. The solution of the perovskite precursor was prepared using the 289 mg PbI₂ and 98 mg methylammonium iodide (MAI) (Lumtec Corp., Taipei, Taiwan) solvent in 500 µL of a dimethyl sulfoxide (DMSO) (Echo Chemical Co., Ltd., Miaoli, Taiwan) and DMF cosolvent with a volume ratio of 1:9 in a glove box that was filled with forming gas of nitrogen. Next, the solution of the perovskite precursor were spin-coated onto the PEDOT:PSS/ITO glass using two-step spin-coating processes with 1000 rpm and 5000 rpm for 10 s and 20 s, respectively. At the second coating step, the said spin-coated layer was suppressed by the dropping 100 µL of anhydrous toluene (Echo Chemical Co., Ltd., Miaoli, Taiwan). Subsequently, the spin-coating process was undertaken and the samples were annealed at temperature 100 °C for 5 min. Afterward, the FAPbX₃ (X = I, Br) (FAPbBr_{1.5}I_{1.5} and FAPbBrI₂) QDs dispersed in chlorobenzene (60 µL) were spin coated onto the above MAPbI₃ perovskite layer at 1000 rpm for 30 s, followed by standing for 2 min, respectively. Finally, a C₆₀ layer (Uni-Onward Corp., New Taipei, Taiwan) and Ag electrode (UMAT Corp., Hsinchu, Taiwan) were thermally formed sequentially by a thermal evaporator method with a high-vacuum ambient of 1.5×10^{-6} torr to finish the device structure. The samples were shielded with a shadow mask during the C₆₀/Ag forming, which define an active area of 0.5×0.2 cm². Figure 1 schematically describes the complete structure. The PEDOT:PSS, MAPbI₃, QD-FAPbX₃, and C₆₀ roles in the device structure are the hole transport layer, light-absorbing layer, absorption enhancement layer, and electron transport layer, respectively

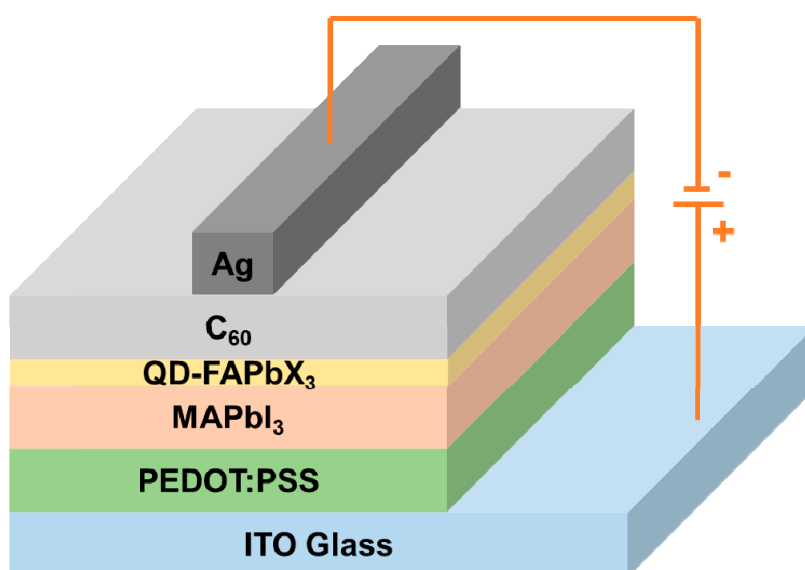


Figure 1. Schematic of the perovskite solar cell device configuration of a structure of ITO/PEDOT:PSS/MAPbI₃/QD-FAPbX₃/C₆₀/Ag.

3. Results and Discussion

Figure 2 shows the TEM (transmission electron microscopy) (Tecnai F30, Philips, Netherlands) images of the QD-FAPbBr_{1.5}I_{1.5} and QD-FAPbBrI₂ thin films. It is clear that the QD-FAPbBr_{1.5}I_{1.5} and QD-FAPbBrI₂ thin films are composed of many quantum dots, in which the quantum dot sizes ranged between 7 nm and 10 nm.

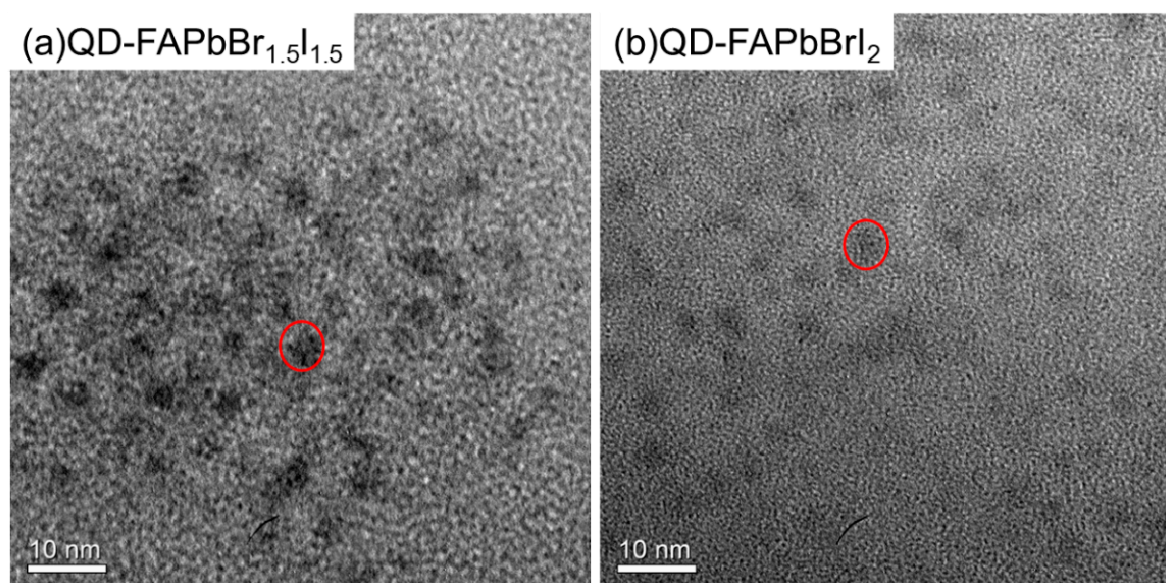


Figure 2. TEM morphological image of perovskite film. (a) QD-FAPbBr_{1.5}I_{1.5} film and (b) QD-FAPbBrI₂ film.

Figure 3 presents the photoluminescence (PL) spectra of the QD-FAPbBr_{1.5}I_{1.5} and QD-FAPbBrI₂ solution were obtained using a photoluminescence system (UniRAM, Protrustech). The QD-FAPbBr_{1.5}I_{1.5} and QD-FAPbBrI₂ peak locations are observed at 680 nm and 730 nm, respectively. This indicated that the band gap of QD-FAPbX₃ can be expected to decrease when the proportion of PbI₂ increases, such that it results in a red shift in the emission peak of the PL spectrum. That is, the observed red shift of the PL emission can be interpreted as a lowering of the

band gap of the QD-FAPbX with a PbI_2 proportion increase. Insets are pictures of the QD-FAPbBr $_{1.5}$ I $_{1.5}$ and QD-FAPbBrI $_2$ specimens that emitted near infrared light while being excited by a 405-nm laser.

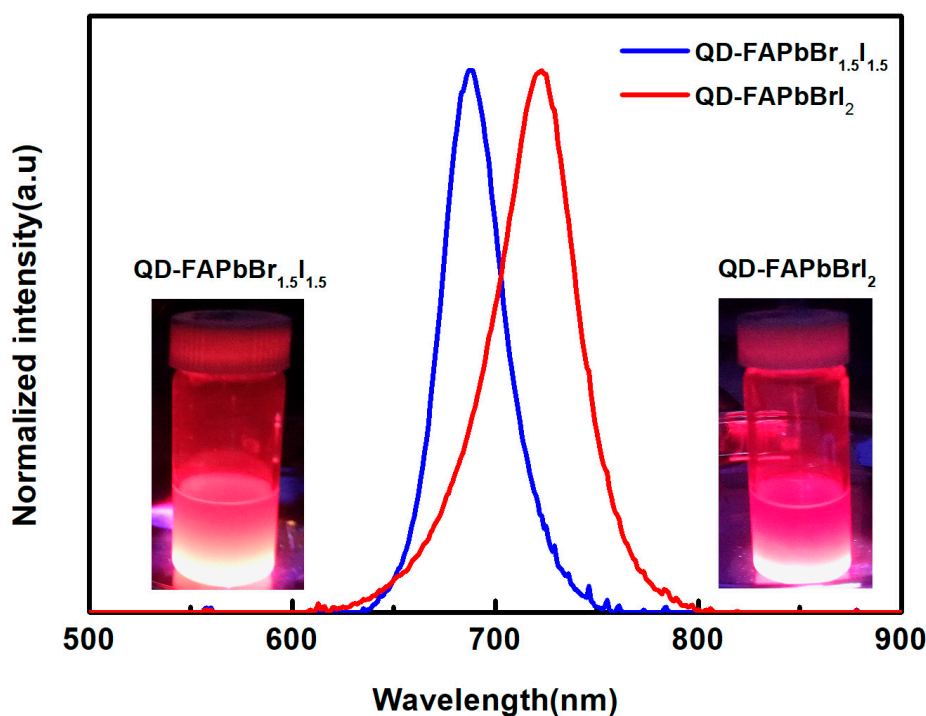


Figure 3. Room-temperature PL spectra of the QD-FAPbBr $_{1.5}$ I $_{1.5}$ and QD-FAPbBrI $_2$ solution. The inset shows the photograph of QD-FAPbBr $_{1.5}$ I $_{1.5}$ and QD-FAPbBrI $_2$ excited by a 405 nm laser.

Figure 4 plots the transmittance and absorbance spectra of MAPbI $_3$, MAPbI $_3$ /QD-FAPbBr $_{1.5}$ I $_{1.5}$, and MAPbI $_3$ /QD-FAPbBrI $_2$ films measured using an UV/VIS/NIR spectrophotometer (U-4100, Hitachi). MAPbI $_3$, MAPbI $_3$ /QD-FAPbBr $_{1.5}$ I $_{1.5}$, and MAPbI $_3$ /QD-FAPbBrI $_2$ films transmittances (see Figure 4a) were below 10% between 300 nm and 700 nm, but above 30% between 750 nm and 850 nm. In particular, the highest value of the transmittance spectrum was above 50% between 780 nm and 850 nm in the MAPbI $_3$ film spectrum on ITO glass. The absorption edge location was at 750 nm, which corresponded to the MAPbI $_3$ film absorption. Figure 4b shows the absorption spectra of the MAPbI $_3$, MAPbI $_3$ /QD-FAPbBr $_{1.5}$ I $_{1.5}$, and MAPbI $_3$ /QD-FAPbBrI $_2$ films. The absorption spectra between 300 nm and 850 nm show that the MAPbI $_3$ /QD-FAPbBrI $_2$ film was higher than that of MAPbI $_3$ and MAPbI $_3$ /QD-FAPbBr $_{1.5}$ I $_{1.5}$ films. One may observe that the MAPbI $_3$ /QD-FAPbBr $_{1.5}$ I $_{1.5}$ and MAPbI $_3$ /QD-FAPbBrI $_2$ films were absorbed with noteworthy between 780 nm and 850 nm, as compared to the MAPbI $_3$ films. This can increase the spectral absorption of the solar cell, thereby generating more short-circuit current density and enhancing the power conversion efficiency.

The electrical J-V (current density-voltage) properties were obtained using a Keithley 2420 sourcemeter under irradiation by a 100 W xenon lamp. The irradiation condition on the sample surface was adjusted at a power density of 100 W/m 2 (AM1.5). Figure 5 presents the relationship between the current density and the voltage (J-V) for MAPbI $_3$, MAPbI $_3$ /QD-FAPbBr $_{1.5}$ I $_{1.5}$, and MAPbI $_3$ /QD-FAPbBrI $_2$ solar cells. Table 2 summaries the performance of the three different solar cells. The MAPbI $_3$ /QD-FAPbBrI $_2$ optimal device demonstrated outstanding performance: power conversion efficiency (Eff) = 7.59%, short-circuit current density (Jsc) = 17.4 mA/cm 2 , open-circuit voltage (Voc) = 0.9 V, and fill factor (FF) = 48.6%. Clearly, the solar cell with the MAPbI $_3$ /QD-FAPbBrI $_2$ perovskite absorber exhibited the greatest increase in absorption, ranging from 300 nm to 850 nm. The cells with the MAPbI $_3$ /QD-FAPbBrI $_2$ and MAPbI $_3$ /QD-FAPbBr $_{1.5}$ I $_{1.5}$ perovskite absorbers exhibited the improved external quantum efficiency (EQE), as shown in Figure 5b. The EQE curves were used to

calculate the integration current of cells based on $\text{MAPbI}_3/\text{QD-FAPbBrI}_2$, $\text{MAPbI}_3/\text{QD-FAPbBr}_{1.5}\text{I}_{1.5}$, and MAPbI_3 were 16.2, 15.8, and 7.9 mA/cm^2 . These values are different from the J_{sc} values that were obtained from J-V curves, which may be due to the samples, has been stored in a N_2 -filled glove box over half a year. This means that the FAPbX_3 perovskite quantum dots coated on MAPbI_3 can increase the short-circuit current. This means that the $\text{MAPbI}_3/\text{QD-FAPbBrI}_2$ perovskite absorber can produce a high-efficiency thin film solar cell.

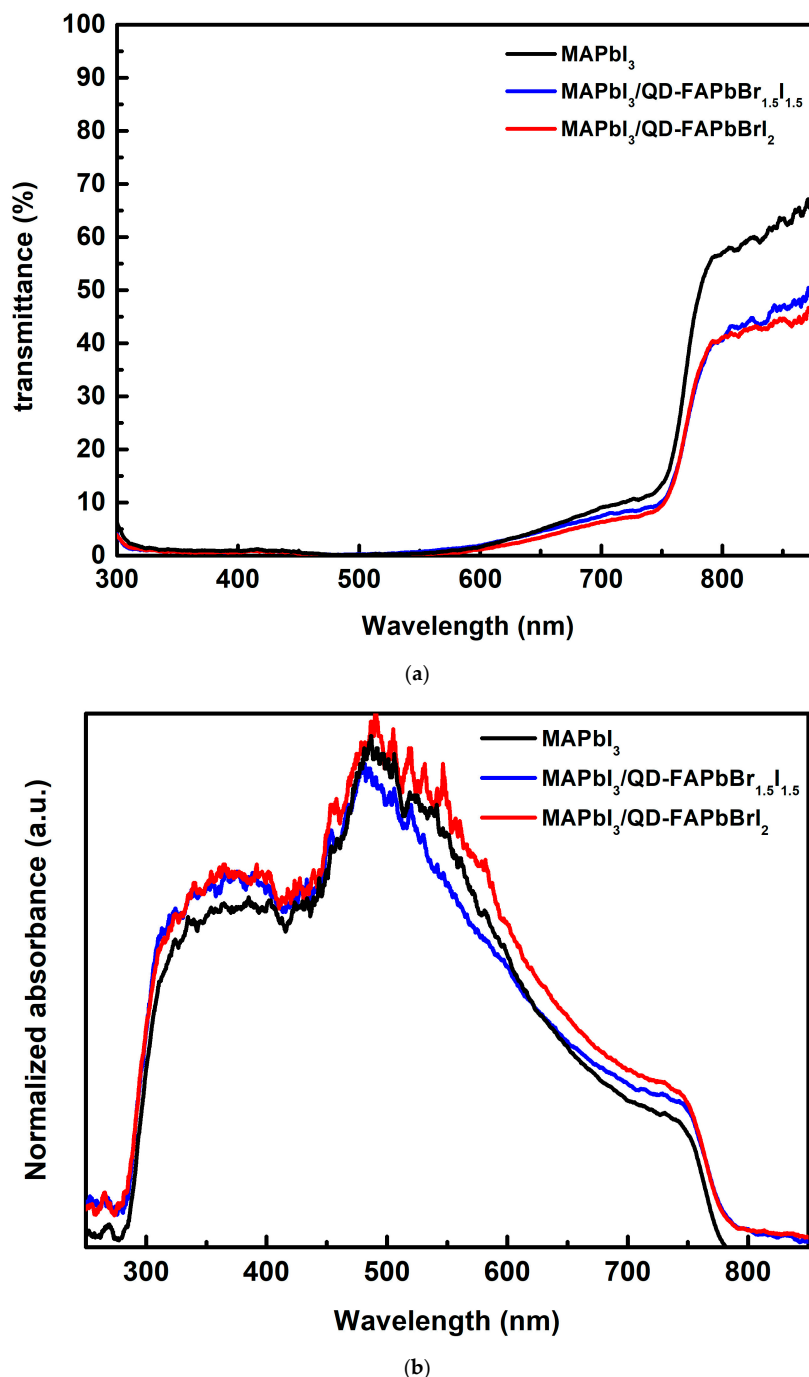


Figure 4. (a) Transmittance and (b) absorbance spectra of the MAPbI_3 , $\text{MAPbI}_3/\text{QD-FAPbBr}_{1.5}\text{I}_{1.5}$, and $\text{MAPbI}_3/\text{QD-FAPbBrI}_2$ films.

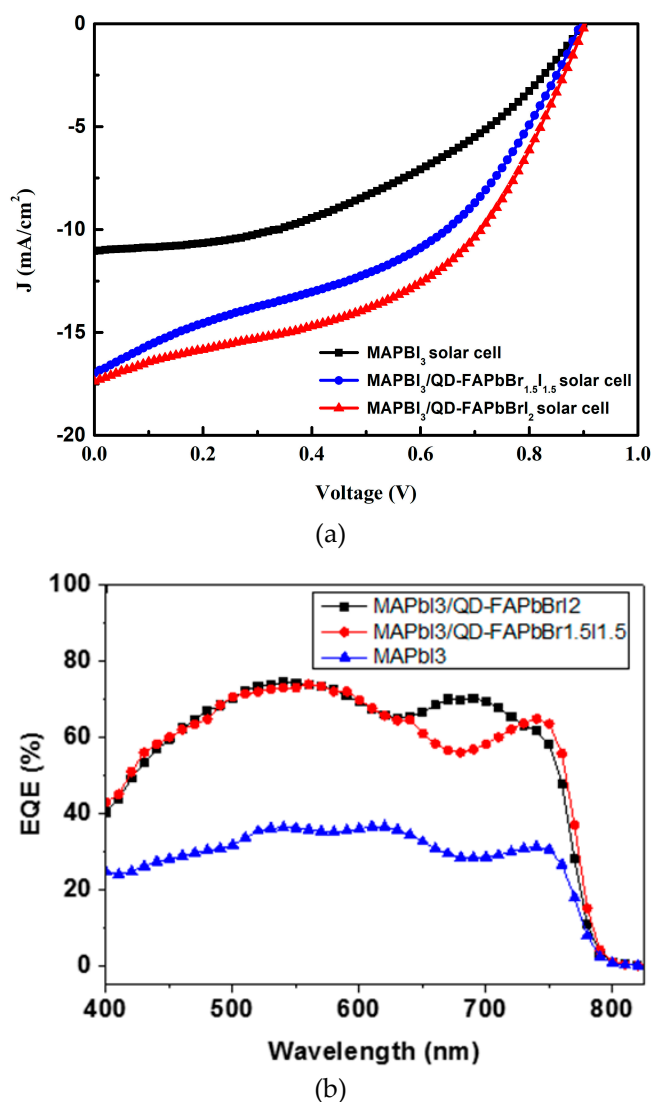


Figure 5. (a) Current density–voltage properties and (b) external quantum efficiency (EQE) spectra of perovskite solar cells.

Table 2. Solar cell photovoltaic parameters. The measurement was carried out under simulated one sun (100 mW/cm^2).

Sample	Voc (V)	Jsc (mA/cm^2)	FF (%)	Eff (%)
MAPbI ₃	0.9	11	53	4.27
MAPbI ₃ /QD-FAPbBr _{1.5} I _{1.5}	0.89	17	43.3	6.54
MAPbI ₃ /QD-FAPbBr ₂	0.9	17.4	48.6	7.59

4. Conclusions

In conclusion, we demonstrated PCE enhancement of the MAPbI₃ perovskite solar cells with FAPbX₃ perovskite quantum dot via increasing the absorption range of the spectral. The PL spectra of the QD-FAPbX₃ indicated a red shift when the proportion of PBI₂ increases due to the band gap decrease. The absorption spectra showed that the MAPbI₃/QD-FAPbX₃ films exhibited broad spectral absorption. The device performance was optimized while using a MAPbI₃/QD-FAPbBr₂ layer, with a short-circuit current density (J_{SC}) = 17.4 mA/cm^2 , open-circuit voltage (V_{OC}) = 0.9 V , fill factor (FF) = 48.6% , and power conversion efficiency (Eff) = 7.59% . The power conversion efficiency of the cell with the MAPbI₃/QD-FAPbX₃ film improved remarkably around 43.7% in the best case.

Author Contributions: L.-C.C. carried out the experiments, designed the study and gave significant suggestions on the writing for the entire manuscript. T.-C.H. and Z.-L.T. helped to analyze and interpret the data, and helped draft the manuscript. R.-J.H. prepared the samples and carried out all measurements. All authors approved this manuscript.

Acknowledgments: This work was supported by the Ministry of Science and Technology (Taiwan, R.O.C.) under Contract No. 106-2221-E-027-091.

Conflicts of Interest: The authors declare no conflict of interest.

References

1. Kojima, A.; Teshima, K.; Shirai, Y.; Miyasaka, T. Organometal halide perovskites as visible-light sensitizers for photovoltaic cells. *J. Am. Chem. Soc.* **2009**, *131*, 6050–6051. [[CrossRef](#)] [[PubMed](#)]
2. Chen, L.C.; Lee, K.L.; Huang, C.Y.; Lin, J.C.; Tseng, Z.L. Preparation and characteristics of MAPbBr₃ perovskite quantum dots on NiOx film and application for high transparent solar cells. *Micromachines* **2018**, *9*, 205. [[CrossRef](#)] [[PubMed](#)]
3. Chen, L.C.; Lee, K.L.; Wu, W.T.; Hsu, C.F.; Tseng, Z.L.; Sun, X.H.; Kao, Y.T. Effect of different CH₃NH₃PbI₃ morphologies on photovoltaic properties of perovskite solar cells. *Nanoscale Res. Lett.* **2018**, *13*, 140. [[CrossRef](#)] [[PubMed](#)]
4. Yang, W.S.; Noh, J.H.; Jeon, N.J.; Kim, Y.C.; Ryu, S.; Seo, J.; Seok, S.I. High-performance photovoltaic perovskite layers fabricated through intramolecular exchange. *Science* **2015**, *348*, 1234–1237. [[CrossRef](#)] [[PubMed](#)]
5. Best Research-Cell Efficiencies, National Renewable Energy Laboratory. Available online: <https://www.nrel.gov/pv/assets/pdfs/pv-efficiencies-07-17-2018.pdf> (accessed on 7 July 2018).
6. Chen, L.C.; Tseng, Z.L.; Chen, S.Y.; Yang, S. An ultrasonic synthesis method for high-luminance perovskite quantum dots. *Ceram. Int.* **2017**, *43*, 16032–16035. [[CrossRef](#)]
7. Park, N.G. Organometal perovskite light absorbers toward a 20% efficiency low-cost solid-state mesoscopic solar cell. *J. Phys. Chem. Lett.* **2013**, *4*, 2423–2429. [[CrossRef](#)]
8. De Wolf, S.; Holovsky, J.; Moon, S.; Loper, P.; Niesen, B.; Ledinsky, M.; Haug, F.J.; Yum, J.H.; Ballif, C. Organometallic halide perovskites: Sharp optical absorption edge and its relation to photovoltaic performance. *J. Phys. Chem. Lett.* **2014**, *5*, 1035–1039. [[CrossRef](#)] [[PubMed](#)]
9. Niv, A.; Abrams, Z.R.; Gharghi, M.; Gladden, C.; Zhang, X. Overcoming the bandgap limitation on solar cell materials. *Appl. Phys. Lett.* **2012**, *100*, 083901. [[CrossRef](#)]
10. Sestu, N.; Cadelano, M.; Sarritzu, V.; Chen, F.P.; Marongiu, D.; Piras, R.; Mainas, M.; Quochi, F.; Saba, M.; Mura, A.; et al. Absorption F-sum rule for the exciton binding energy in methylammonium lead halide perovskites. *J. Phys. Chem. Lett.* **2015**, *6*, 4566–4572. [[CrossRef](#)] [[PubMed](#)]
11. Galkowski, K.; Mitioglu, A.; Miyata, A.; Plochocka, P.; Portugall, O.; Eperon, G.E.; Wang, J.T.W.; Stergiopoulos, T.; Stranks, S.D.; Snaith, H.J.; et al. Determination of the exciton binding energy and effective masses for methylammonium and formamidinium lead tri-halide perovskite semiconductors. *Energy Environ. Sci.* **2016**, *9*, 962–970. [[CrossRef](#)]
12. Stranks, S.D.; Eperon, G.E.; Grancini, G.; Menelaou, C.; Alcocer, M.J.P.; Leijtens, T.; Herz, L.M.; Petrozza, A.; Snaith, H.J. Electron-hole diffusion lengths exceeding 1 micrometer in an organometal trihalide perovskite absorber. *Science* **2015**, *342*, 341–344. [[CrossRef](#)] [[PubMed](#)]
13. Nedelcu, G.; Protesescu, L.; Yakunin, S.; Bodnarchuk, M.I.; Grotevent, M.J.; Kovalenko, M.V. Fast anion-exchange in highly luminescent nanocrystals of cesium lead halide perovskites (CsPbX₃, X=Cl, Br, I). *Nano Lett.* **2015**, *15*, 5635–5640. [[CrossRef](#)] [[PubMed](#)]
14. Lin, C.H.; Zeng, Q.J.; Lafalce, E.; Yu, S.T.; Smith, M.J.; Yoon, Y.J.; Chang, Y.J.; Jiang, Y.; Lin, Z.Q.; Vardeny, Z.V.; et al. Large-area lasing and multicolor perovskite quantum dot patterns. *Adv. Opt. Mater.* **2018**, *6*, 1800474. [[CrossRef](#)]
15. Zhang, Y.W.; Wu, G.; Dang, H.; Ma, K.Z.; Chen, S. Multicolored mixed-organic-cation perovskite quantum dots (FA_xMA_{1-x}PbX₃, X = Br and I) for white light-emitting diodes. *Ind. Eng. Chem. Res.* **2017**, *56*, 10053–10059. [[CrossRef](#)]
16. Im, J.H.; Lee, C.R.; Lee, J.W.; Park, S.W.; Park, N.G. 6.5% efficient perovskite quantum-dot-sensitized solar cell. *Nanoscale* **2011**, *3*, 4088–4093. [[CrossRef](#)] [[PubMed](#)]

17. Zhang, X.L.; Eperon, G.E.; Liu, J.H.; Johansson, E.M.J. Semitransparent quantum dot solar cell. *Nano Energy* **2016**, *22*, 70–78. [[CrossRef](#)]
18. Zhang, X.L.; Hagglund, C.; Johansson, E.M.J. Highly efficient, transparent and stable semitransparent colloidal quantum dot solar cells: A combined numerical modeling and experimental approach. *Energy Environ. Sci.* **2017**, *10*, 216–224. [[CrossRef](#)]
19. Ghosh, D.; Ali, M.Y.; Chaudhary, D.K.; Bhattacharyya, S. Dependence of halide composition on the stability of highly efficient all-inorganic cesium lead halide perovskite quantum dot solar cells. *Sol. Energy Mater. Sol. Cells* **2018**, *185*, 28–35. [[CrossRef](#)]
20. Han, J.H.; Luo, S.P.; Yin, X.W.; Zhou, Y.; Nan, H.; Li, J.B.; Li, X.; Oron, D.; Shen, H.P.; Lin, H. Hybrid PbS quantum-dot-in-perovskite for high-efficiency perovskite solar cell. *Small* **2018**, *14*, 1801016. [[CrossRef](#)] [[PubMed](#)]



© 2019 by the authors. Licensee MDPI, Basel, Switzerland. This article is an open access article distributed under the terms and conditions of the Creative Commons Attribution (CC BY) license (<http://creativecommons.org/licenses/by/4.0/>).